

Research Article

Exploring age-related changes in bone and muscle: Insights from radiomics and MRI

Maryam Elikaei Moghadam^a, Elmira Yazdani^a, Mohammad Bagher Shiran^{a,*},
Shahrokh Abbasi-Rad^{b,c,d}, Hamidreza Saligheh Rad^{d,e} and Malakeh Malekzadeh^{a,e,*}

^a Medical Physics Department, School of Medicine, Iran University of Medical Sciences, Tehran, Iran

^b Department of Radiology, Harvard Medical School, Boston, Massachusetts, USA

^c Athinoula A. Martinos Center for Biomedical Imaging, Massachusetts General Hospital, Charlestown, Massachusetts, USA

^d Medical Physics and Biomedical Engineering Department, Tehran University of Medical Sciences, Tehran, Iran

^e Quantitative MR Imaging & Spectroscopy Group (QMISG), Tehran University of Medical Sciences (TUMS), Tehran, Iran

ABSTRACT

Background: Age-related changes in muscle and bone can adversely affect musculoskeletal health. Current techniques often fail to capture subtle age-related changes in bone micro-architecture and muscle tissue. Magnetic resonance imaging (MRI) is a robust tool for analyzing age-related bone deterioration, while radiomics effectively captures subtle changes in muscle tissue by extracting intricate features.

Purpose: This study investigates the relationship between radiomic features from calf muscles and tibial cortical bone free water T_1 with age.

Materials and Methods: A cross-sectional MRI study was conducted with 34 healthy volunteers aged 30 to 62 years. Calf muscles were manually segmented under expert radiologist supervision, and 108 radiomics features were extracted from anterior, posterior, and lateral muscle groups using LIFEx software. Cortical bone free water T_1 , a surrogate measure of cortical porosity and age-related deterioration, was quantified. The Spearman coefficient test was used to analyze correlations between cortical bone, radiomic features, and age.

Results: Significant correlations were observed between radiomic features of leg muscles and both age and cortical bone free water T_1 values. Age-related variations were particularly evident in texture-based

features, including the histogram, Neighborhood Gray-Level Different Matrix, Gray Level Run Length Matrix, Gray Level Co-occurrence Matrix, and Intensity ($r > 0.4$, $p < 0.01$).

Conclusion: This study demonstrates the utility of MR-based radiomics for capturing age-related changes in cortical bone and surrounding muscle groups in the lower extremities among healthy adults. The findings underscore the potential of radiomics to monitor early musculoskeletal changes associated with aging, with implications for risk stratification and preventative care.

RÉSUMÉ

Contexte: Les modifications liées à l'âge des muscles et des os peuvent altérer la santé musculosquelettique. Les techniques actuelles ne parviennent souvent pas à détecter les changements subtils liés à l'âge dans la micro-architecture osseuse et les tissus musculaires. L'imagerie par résonance magnétique (IRM) constitue un outil robuste pour l'analyse de la détérioration osseuse liée à l'âge, tandis que la radiomique permet de capturer des variations fines du tissu musculaire en extrayant des caractéristiques complexes.

Objectif: Cette étude vise à évaluer la relation entre les caractéristiques radiomiques des muscles du mollet et le T_1 de l'eau libre de l'os cortical tibial en fonction de l'âge.

Contributors: All authors contributed to the conception or design of the work, the acquisition, analysis, or interpretation of the data. All authors were involved in drafting and commenting on the paper and have approved the final version.

Funding: This study did not receive any specific grant from funding agencies in the public, commercial, or notfor-profit sectors.

Competing interests: All authors declare no conflict of interest.

Ethical approval: The patient data for this research was gathered retrospectively with ethical approval from a previous project. Therefore, the Ethics Committee of IUMS exempted it from further ethics approval under IR.IUMS.FMD.REC.1401.505.

* Corresponding authors at: Tehran Hemat Highway next to Milad Tower 14535, Iran University of Medical Sciences, Tehran, Iran.

E-mail addresses: elikaeimaryam73@gmail.com (M.E. Moghadam), yazdani.el@iums.ac.ir (E. Yazdani), Shiran.m@iums.ac.ir (M.B. Shiran), sabbasi-rad@mgh.harvard.edu (S. Abbasi-Rad), h-salighehrad@tums.ac.ir (H.S. Rad), mmalekzadeh@coh.org (M. Malekzadeh).

Matériels et méthodes: Une étude IRM transversale a été réalisée chez 34 volontaires sains âgés de 30 à 62 ans. Les muscles du mollet ont été segmentés manuellement sous la supervision d'un radiologue expert, et 108 caractéristiques radiomiques ont été extraites des groupes musculaires antérieur, postérieur et latéral à l'aide du logiciel LIFEx. Le T1 de l'eau libre de l'os cortical, considéré comme un marqueur indirect de la porosité corticale et de la détérioration liée à l'âge, a été quantifié. Le coefficient de corrélation de Spearman a été utilisé pour analyser les relations entre l'os cortical, les caractéristiques radiomiques et l'âge.

Résultats: Des corrélations significatives ont été observées entre les caractéristiques radiomiques des muscles de la jambe, l'âge et les valeurs de T1 de l'eau libre de l'os cortical. Les variations liées à l'âge étaient particulièrement marquées pour les caractéristiques de texture,

Keywords: Musculoskeletal imaging; Radiomics; Cortical bone; Free water

Introduction

The aging demographic confronts substantial health challenges, notably osteoporosis and sarcopenia, characterized by the progressive decline of bone and muscle mass, respectively [1-5]. Recent research highlights the influence of common chemical and mechanical communication mechanisms on aging-related bone and muscle decline [6].

Skeletal muscle undergoes notable structural and functional decline with aging, becoming smaller, weaker, and slower over time [7-9]. On average, adults experience a 3–5 % reduction in muscle mass per decade after the age of 30, culminating in a 10–24 % loss by ages 65–70, and up to 30–50 % by age 80 and beyond [2,10–12]. Parallel to muscular changes, aging is associated with increased cortical bone porosity and decreased cortical thickness, leading to compromised bone strength and greater susceptibility to fractures [13,14].

The lower extremity is a crucial anatomical region for assessing bone porosity and muscle characteristics. It features bones with thick cortical bone and substantial muscle mass, such as the soleus and gastrocnemius, which are particularly susceptible to various pathological conditions and aging-related changes [1,3]. Given the interplay between muscle and bone tissue, examining the characteristics of bones and adjacent muscle groups in the lower leg presents new insights into the intricate relationship between muscle and bone throughout the aging process. However, existing studies have largely examined bone and muscle independently, limiting our understanding of their integrated aging trajectories.

Regarding investigation of bone health, most studies have focused on bone mass. Specifically, bone health assessments have traditionally relied on measurements of bone mineral density (BMD), measured by dual-energy x-ray absorptiometry (DEXA). However, a significant proportion of non-vertebral fractures in adults over 55 occur in individuals who do not meet the diagnostic criteria for osteoporosis based on BMD alone [15]. This highlights the importance of considering additional

notamment l'histogramme, la matrice de différences de niveaux de gris de voisinage, la matrice de longueur de parcours des niveaux de gris, la matrice de cooccurrence des niveaux de gris et les paramètres d'intensité ($r > 0.4$; $p < 0,01$).

Conclusion: Cette étude démontre l'intérêt de la radiomique basée sur l'IRM pour la détection des changements liés à l'âge de l'os cortical et des groupes musculaires adjacents des membres inférieurs chez des adultes en bonne santé. Ces résultats soulignent le potentiel de la radiomique pour le suivi précoce des modifications musculosquelettiques associées au vieillissement, avec des implications pour la stratification du risque et la prévention.

Mots-clés: imagerie musculosquelettique, radiomique, IRM quantitative, vieillissement, os cortical, eau libre.

factors beyond BMD in determining bone quality and strength. Cortical microarchitecture, particularly porosity, plays a crucial role in overall bone health, but has not been thoroughly investigated due to the lack of a clinically available technique for its evaluation [16].

Since magnetic resonance imaging (MRI) is sensitive to protons existing in the microenvironment of the tissues, it is a good candidate for studying bone beyond its mass [17]. The porous media in cortical bone are filled with fluids, primarily water. Therefore, cortical bone free water, measurable by MRI, has been suggested as a surrogate measure of porosity [18]. Akbari et al. proposed a clinically compatible MR-based technique to measure cortical bone free water longitudinal relaxation time (T_1) and demonstrated its potential for predicting the age-related deterioration of bone [1]. It was also shown that cortical bone mechanical competence can be accessed through cortical bone free water relaxometry [19]. Based on this evidence, in this study, we selected MRI over X-Ray-based modalities to leverage its ability to provide more comprehensive information about bone microstructure.

In contrast, assessments of muscle aging have primarily focused on the impact of aging on type II muscle fibers [20], with relatively limited investigation into changes in type I muscle fibers. While conventional muscle MRI provides valuable information on muscle size, volume, fat infiltration, and edema [21,22], many age-related changes at the muscular structure level remain imperceptible, even to experienced radiologists to detect from the acquired MR images. Radiomics offers a solution to this challenge by enabling the extraction of intricate and high-dimensional, quantitative features from medical images that are imperceptible by well-trained eyes [23]. These features reflect tissue heterogeneity and sub-visual characteristics. Radiomics uses advanced mathematical modeling to extract quantitative measures from the invisible tissue infrastructural components of the image so to mitigate the subjective nature of image interpretation [24,25].

Despite the increasing recognition of muscle–bone interactions, few studies have examined the relationship between muscle radiomic features and bone microarchitecture in the context of aging. To address this gap, we conducted a cross-sectional study in healthy volunteers aged 30 to 62 years, integrating quantitative MRI measurements of tibial cortical bone free water with radiomic features extracted from adjacent calf muscle groups. This approach aims to advance our understanding of musculoskeletal aging by simultaneously characterizing muscle and bone changes within the same anatomical region.

Materials and methods

Participants

A total of 34 healthy volunteers (15 males and 19 females), aged between 30 and 62 years, were recruited for this study and underwent MRI examinations conducted between 2008

and 2019. This age range was selected to capture early and mid-life musculoskeletal aging, during which microstructural changes in muscle and cortical bone begin to develop but often remain clinically silent. Individuals older than 62 years were not included to minimize confounding effects related to age-associated comorbidities, advanced sarcopenia, osteoporosis, or degenerative conditions that may obscure subtle age-dependent imaging biomarkers. Individuals with medical histories indicating musculoskeletal disorders, prior surgeries, or treatments known to affect bone or muscle health, such as glucocorticoid therapy or antiepileptic medication, were excluded from participation [26]. The local Ethics Committee approved the study protocol, and all participants provided informed consent. Detailed demographic characteristics of the study cohort are presented in Table 1.

Fig. 1 provides a schematic overview of the radiomics workflow employed in this study. The diagram outlines the sequential steps beginning with MRI image acquisition, followed by

Table 1

Demographic characteristics of study participants. Age, weight, height, and body mass index (BMI) are presented as mean \pm standard deviation (SD).

Participants	Age (yr)	Weight (Kg)	Height (cm)	BMI (Kg/m ²)
Healthy Volunteers	44.20 \pm 7.96	75.08 \pm 12.45	1.68 \pm 0.09	26.27 \pm 2.71

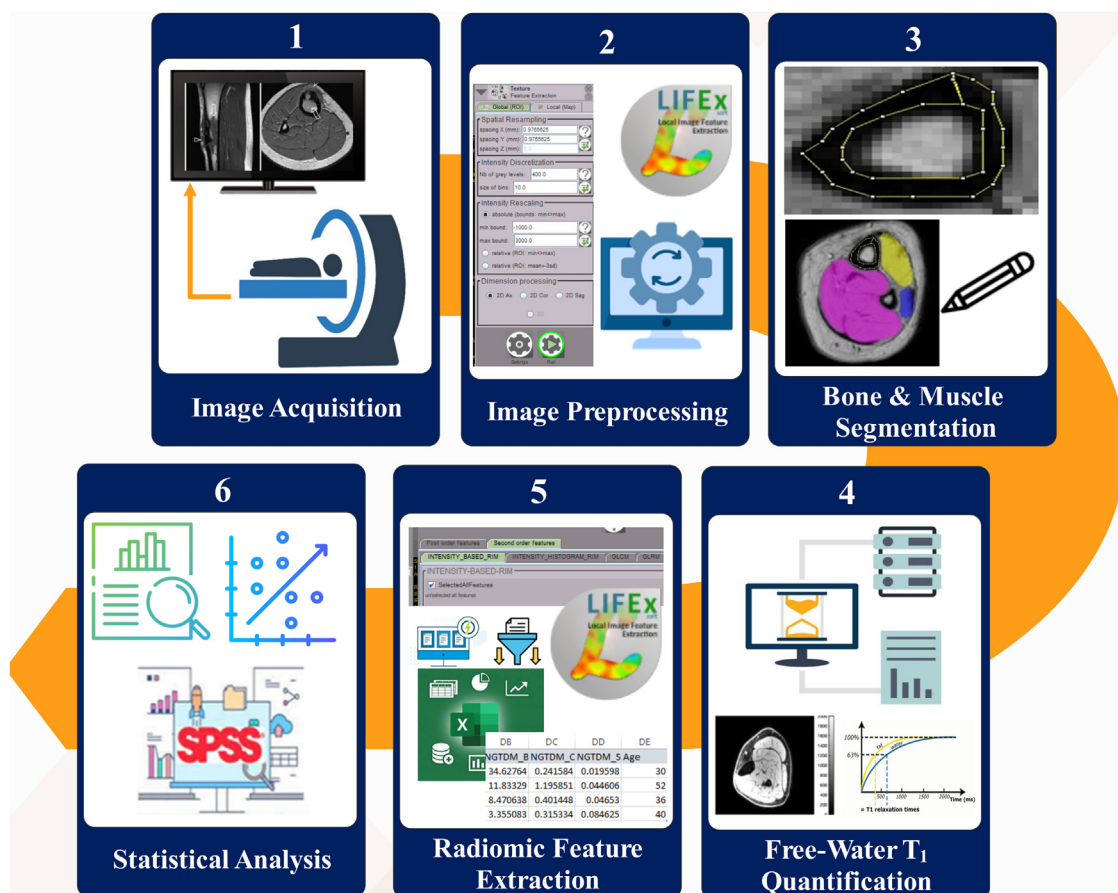


Fig. 1. Overview of the radiomics workflow used in this study. The pipeline includes MRI image acquisition, preprocessing, manual segmentation of calf muscle groups, feature extraction using LIFEx software, and subsequent statistical analysis to investigate correlations between muscle radiomic features, cortical bone free water T₁, and age.

preprocessing, manual segmentation of bone and muscle regions, and the extraction of quantitative features using LIFEx software [27]. The workflow proceeds through statistical analysis and correlation assessment to identify age-related radiomic and cortical bone changes. Each component of the pipeline is elaborated upon in the subsequent sections of the manuscript.

Image acquisition

MR imaging was conducted using a 1.5T MR scanner (Siemens, Magnetom Avanto) equipped with an eight-channel knee coil for signal reception. The imaging site on the lower extremity was precisely chosen to correspond to 38 % of the tibial length, measured proximally from the medial malleolus, a location known to correspond with maximal cortical thickness. Two distinct series of images were acquired using identical imaging parameters, differing only in repetition time (TR): 20 ms for the first series, and 60 ms for the second. These TR values were selected based on prior studies demonstrating improved tissue contrast and sensitivity to age-related variations in cortical bone and muscle. The shorter TR (20 ms) enables rapid acquisition, while the longer TR (60 ms) enhances sensitivity to subtle cortical bone relaxation differences. Together, this dual-TR protocol improves sensitivity to cortical bone free-water-related T₁ differences while maintaining clinically feasible scan times and has been validated for assessing age-related bone changes [1-5]. Both series utilized a 3D gradient-echo fast low angle shot (FLASH) sequence with a short time of echo (STE). Imaging parameters were as follows: TR₁/TR₂/TE = 20/60/1.29 ms, field-of-view (FOV) = 267 × 267 mm², spatial resolution = 0.8 × 0.8 mm², slice thickness = 5 mm, flip angle = 20°, readout bandwidth = 781 Hz/Pix, number of slices = 10. The total scan duration was approximately 20 min. This imaging protocol has been previously validated and described in detail in the literature [10].

Cortical bone segmentation

Cortical bone segmentation was performed on T₁ images, focusing on the central five slices for each of the 34 participants. Manual delineation of cortical bone pixels was conducted using polygonal regions of interest (ROIs) drawn in ImageJ software (version 1.52v; National Institutes of Health, USA), under the supervision of an experienced bone imaging researcher, as illustrated in Fig. 2. To reduce segmentation variability and mitigate misclassification of cortical bone pixels as marrow or connective tissue, the segmentation procedure was repeated three times. The resulting delineations were used to calculate the mean signal intensity across all identified cortical bone regions and reported as the singular mean signal intensity, representing the entire cortical bone tissue within each slice.

Free water T₁ quantification

Free water T₁ values were computed through a multi-step process. Initially, the mean signal intensity of the segmented

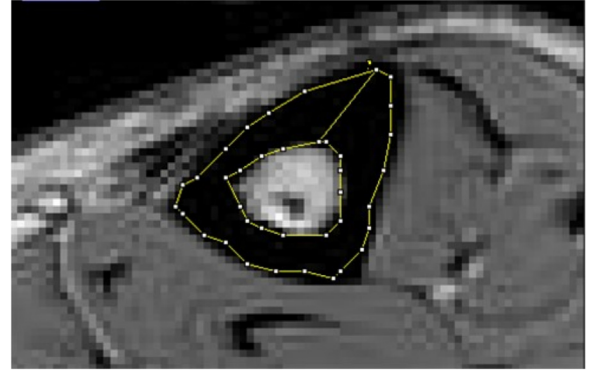


Fig. 2. Manual segmentation of tibial cortical bone on short echo time magnetic resonance (STE-MR) images using ImageJ (v1.52v) software.

cortical bone from the long repetition time (TR₂) image was divided by that from the short repetition time (TR₁) image. Subsequently, the cortical bone free water T₁ value for each slice was calculated by solving Eq. (1) [1].

$$r = \frac{S_{GE1}}{S_{GE2}} = \frac{1 - \exp\left(-\frac{TR_1}{T_1}\right)}{1 - f_z \exp\left(-\frac{TR_1}{T_1}\right)} / \frac{1 - \exp\left(-\frac{TR_2}{T_1}\right)}{1 - f_z \exp\left(-\frac{TR_2}{T_1}\right)} \quad (1)$$

This procedure was repeated across all segmented slices for each participant to derive slice-specific T₁ values. Finally, the T₁ values obtained from all slices were averaged to determine the subject-specific cortical bone free water longitudinal relaxation time.

In Eq. (1), f_z represents a function of the ratio τ/T_2^* , where τ represents the pulse duration and T_2^* is the transverse relaxation time of cortical bone. This function serves as a correction factor that accounts for relaxation losses occurring during the radiofrequency (RF) excitation period. A T_2^* value of 2.81 ms for cortical bone free water was adopted, consistent with the previous study [10].

Muscles segmentation

ROIs were manually delineated using the Local Image Feature Extraction (LIFEx) software, version 7.2.0 [27]. In consultations with an experienced anatomist, a standardized approach to manual segmentation was implemented. The ROIs encompassed three anatomical compartments of the calf, as depicted in Fig. 3:

- I. Anterior compartment: Comprised of the tibialis anterior, extensor hallucis longus, extensor digitorum longus, and fibularis tertius muscles (shown in yellow).
- II. Posterior compartment: Included the gastrocnemius, soleus, plantaris, popliteus, flexor digitorum longus, flexor hallucis longus, and tibialis posterior muscles (shown in purple).

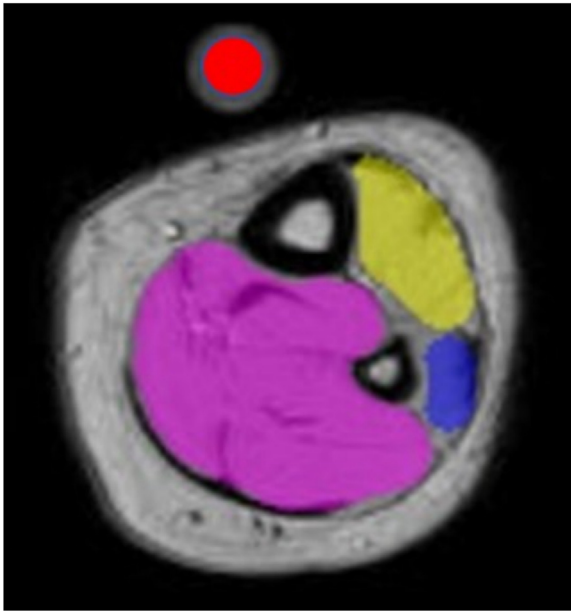


Fig. 3. Magnetic resonance imaging (MRI) scan of the distal tibia at 38 % of the tibial length, illustrating the posterior, lateral, and anterior compartments of the calf muscle, along with the water phantom for reference. The regions are color-coded in purple, blue, yellow, and red, respectively.

III. Lateral compartment: Consisted of the fibularis longus and brevis muscles (shown in blue).

Fig. 3 also displays the water phantom (red) used as a reference in the imaging setup.

This rigorous methodology ensured precise representation and analysis of the distinct muscle compartments within the calf. For each participant, five central slices were selected from a set of ten. To ensure uniformity in analysis, the ROI for each subject comprised the largest area covering leg muscles while excluding subcutaneous fat. This selection criterion effectively eliminated peripheral regions, thereby minimizing texture variability arising from partial volume effects or voxel contamination from adjacent tissues. The ROI size varied between 540 and 33,400 voxels, reflecting differences in compartmental volume. The averaging process was then systematically applied to these five slices, yielding a unified and precise representation of calf muscle segmentation. To enhance reliability, the manual segmentation procedure was performed in triplicate, and the resulting segmentations were averaged for final analysis. This approach was used to reduce intra-observer variability and to improve both accuracy and reproducibility in the quantification of muscle characteristics.

Radiomic features extraction

Following the segmentation step, texture analysis was performed on the T_1 -weighted images using the LIFEx software (version 7.2.0) [27]. Prior to the feature extraction, three pre-processing steps were applied through the Global (ROI) menu of LIFEx: spatial resampling along the two Cartesian axes (spac-

ing $X = 1 \text{ mm}$, spacing $Y = 1 \text{ mm}$), intensity discretization with a bin size of 128, and relative intensity rescaling within specified minimum and maximum bounds. Radiomic features were subsequently extracted from the three delineated calf muscle compartments, including:

1. First-order features:

- Morphological features ($n = 15$): These features characterize the geometry and shape of the ROI, including metrics such as volume, surface area, compactness, sphericity, and elongation [28,29]. These features offer valuable insights into the structural characteristics of tissue and are helpful in detecting abnormalities within the images.
- Intensity histogram features ($n = 30$): These intensity-based statistical features, including mean, standard deviation, skewness, kurtosis, entropy, percentiles, and energy, are derived from the histogram of pixel intensities within the ROI. They provide comprehensive information about the overall intensity distribution, facilitating characterization of tissue properties and detection of subtle changes in the images.
- Intensity-based statistics features ($n = 23$): These features are derived directly from the raw intensity values of the voxels within the ROI, rather than from the histogram. They include metrics such as mean, standard deviation, coefficient of variation, range, interquartile range, robust mean intensity, and median intensity. These features are computed using advanced mathematical formulations and provide detailed quantitative information about the distribution and variability of signal intensity within the tissue.

2. Second-order features:

- Gray-Level Co-Occurrence Matrix (GLCM) features ($n = 24$): These features are derived from a co-occurrence matrix that quantifies the spatial relationships between neighboring voxels based on the frequency of specific gray-level pairings within the ROI. From this matrix, a range of texture descriptors, such as contrast, energy, homogeneity, entropy, and correlation, are computed. GLCM features effectively capture complex textural patterns and are particularly valuable for analyzing tissue heterogeneity in MR images [25,30,31].
- Gray Level Run Length Matrix (GLRLM) features ($n = 11$): These features are derived from a run-length matrix that captures the length and distribution of homogeneous runs, defined as consecutive voxels with the same gray-level intensity, within the ROI. From this matrix, 11 texture metrics are calculated, such as short run emphasis, run length non-uniformity, run entropy, and low gray-level run emphasis. GLRLM

features provide valuable information about tissue heterogeneity and the spatial organization of intensity variations within the selected ROI [25,30,31].

- **Neighboring Gray Tone Difference Matrix (NGLDM) features ($n = 5$):** NGTDM features are calculated by comparing the gray-level intensity of a central voxel with the average intensity of its neighboring voxels within a predefined window. This process yields a matrix from which five key texture features are extracted: coarseness, contrast, busyness, complexity, and strength. These features are particularly useful for characterizing local texture properties, offering sensitive measures of microstructural variation and heterogeneity within the tissue [25,30,31].

A total of 108 quantitative radiomic features were extracted from each segmented compartment. The complete list of extracted features is provided in Supplementary Table S1

In this study, the term “radiomic features” refers to the full set of quantitative features extracted from medical images, while “texture features” specifically denote the texture-based radiomic descriptors derived from the GLCM, GLRLM, and NGTDM.

Radiomic features reproducibility

A water phantom was positioned adjacent to the patient’s leg (Fig. 3, as seen in red color) to evaluate the reproducibility of the radiomics features, focusing on the segmented area of the phantom. Features were extracted from this region in two separate instances. By maintaining consistent positioning of the phantom across all participants, the extracted radiomics features were employed to evaluate reproducibility within the scope of the study objectives.

Statistical analyses

Data analysis was conducted using the Statistical Package for the Social Sciences (SPSS) software (version 26) and R software (R Development Team, 2018). The Spearman rank correlation coefficient was used to evaluate the correlation between cortical bone free water T_1 and the radiomics features of calf muscles, as well as their correlation with age. The Spearman correlation was chosen because the data did not meet the assumptions of normality, as confirmed by the Shapiro-Wilk test. Since Spearman’s correlation is a non-parametric method, it is appropriate for identifying monotonic relationships between variables without requiring normally distributed data. To control for multiple comparisons, the Benjamini-Hochberg procedure was applied, with statistical significance set at $p < 0.05$.

Additionally, to assess the repeatability and robustness of radiomic features, intra-class correlation coefficients (ICC) and coefficient of variation percentage (CV %) were calculated. ICC values were interpreted according to commonly used criteria, where values below 0.50 indicate poor reproducibility, 0.50–0.75 moderate reproducibility, 0.75–0.90 good reproducibility, and values greater than 0.90 excellent reproducibility.

Results

At baseline, significant associations were observed between age and muscle texture parameters across the three calf compartments. Among the 108 radiomic features extracted from the anterior, posterior, and lateral compartments, 21, 14, and 30 features, respectively, demonstrated statistically significant correlations with age (Spearman’s $r > 0.4$, $p < 0.05$).

Fig. 4 illustrates texture features exhibiting moderate to strong correlations ($r > 0.5$) with age. In the posterior compartment, consisting of the soleus and the gastrocnemius muscles, several intensity-based and texture features showed significant positive correlations with age: Intensity-based Interquartile Range ($r = 0.504$, $p < 0.001$; Fig. 4a), Intensity-based Robust Mean Absolute Deviation ($r = 0.502$, $p < 0.001$; Fig. 4b), GLCM Inverse Variance ($r = 0.503$, $p < 0.001$; Fig. 4c), and GLRLM Short Runs Emphasis ($r = 0.567$, $p < 0.001$; Fig. 4e). Conversely, the GLCM Correlation feature exhibited a significant negative correlation with age ($r = -0.653$, $p < 0.001$; Fig. 4d). Within the lateral muscle group, comprising the fibularis longus and brevis muscles, the GLRLM Long Runs Emphasis ($r = -0.532$, $p < 0.001$; Fig. 4f) and GLRLM Long Run Low Gray Level Emphasis ($r = -0.586$, $p < 0.000$; Fig. 4g) were significantly negatively correlated with age.

An analysis of the relationship between muscle and bone revealed modest but statistically significant correlations (Spearman’s $r \approx 0.4$, $p < 0.05$) between cortical bone free water T_1 values and radiomic features extracted from the anterior, posterior, and lateral muscle compartments, comprising 24, 12, and 25 features, respectively.

Texture features with moderate to strong correlations ($r > 0.5$), are shown in Fig. 5. In the posterior muscles, the GLCM Correlation feature showed a strong negative correlation with cortical bone free water T_1 ($r = -0.685$, $p < 0.001$; Fig. 5a), consistent with its significant correlation with age. Within the lateral muscle group, the GLRLM Long Run Low Gray Level Emphasis ($r = -0.542$, $p < 0.001$; Fig. 5b) and the GLRLM Long Runs Emphasis ($r = -0.509$, $p < 0.001$; Fig. 5c) were also significantly correlated with cortical bone free water T_1 .

The ICC analysis demonstrated good to excellent reproducibility across feature groups, with GLCM features exhibiting an ICC of 83 % (good), GLRLM features 72 % (moderate), and NGTDM features 89 %. In contrast, intensity-based features showed a lower ICC of 24 % (poor). Importantly, among the intensity-based features, four exhibited significant correlations with both age and cortical bone free water T_1 ; their respective coefficients of variation (CV %) are presented in Table 2. The CV % values indicate excellent repeatability, with the Interquartile Range feature showing no variability (0 %), and the 90th Percentile and Mean Absolute Deviation features exhibiting low variability at 1.92 %. The Robust Mean Absolute Deviation displayed slightly higher variability at 3.14 %, yet remains within an acceptable range for reproducibility.

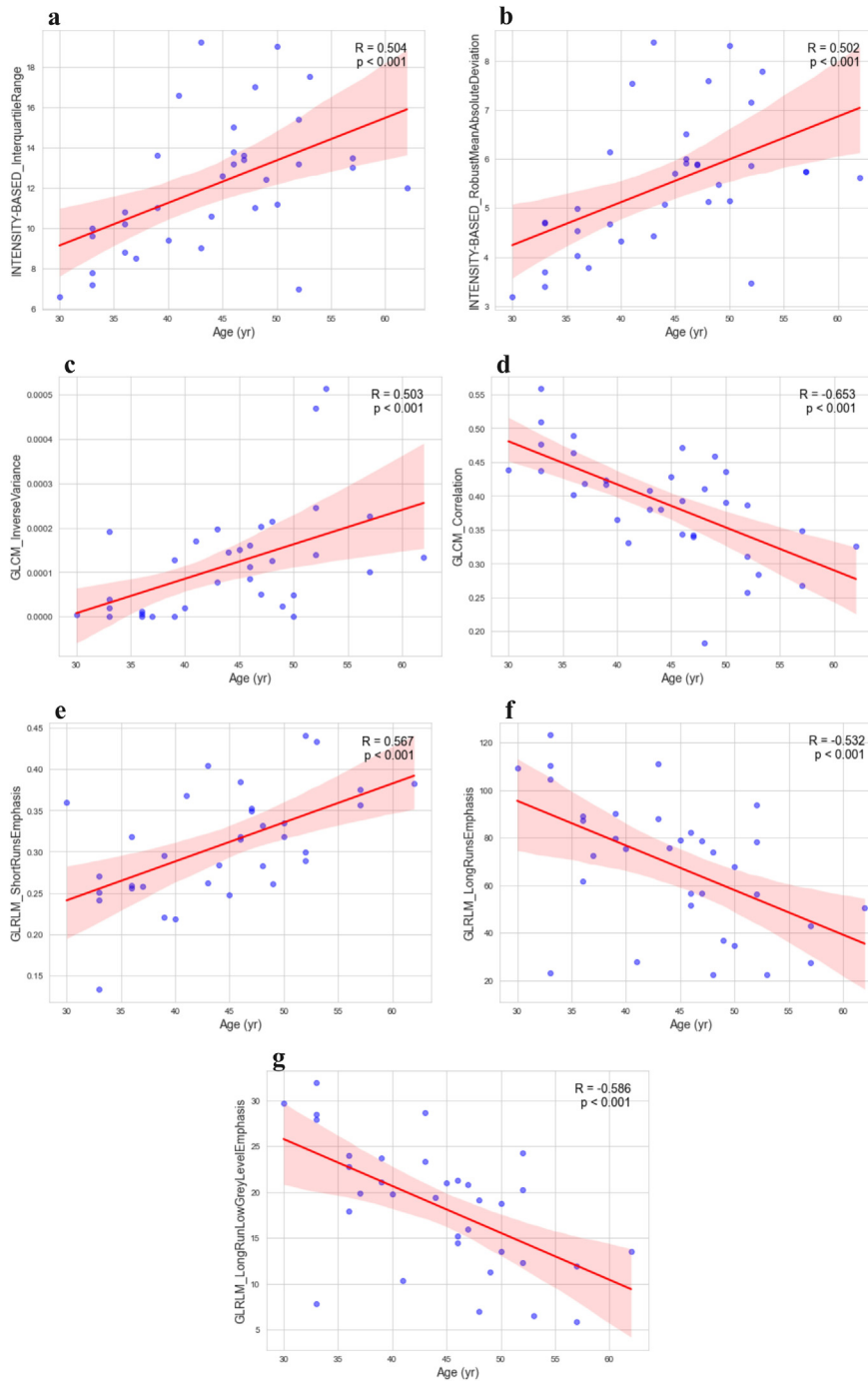


Fig. 4. Correlation of significant texture-based features in the leg muscle with Age. (a) INTENSITY-BASED_InterquartileRange, (b) INTENSITY-BASED_Robust Mean Absolute Deviation, (c) Gray level co-occurrence matrix (GLCM)_ Inverse Variance, (d) GLCM-correlation, (e) Gray Level Run Length Matrix (GLRLM) Short Runs Emphasis, (f) GLRLM_Long Runs Emphasis, and (g) GLRLM_Long Run Low Gray Level Emphasis.

Discussion

Radiomics has demonstrated significant potential in various medical domains, including oncology and neurology, due to its ability to extract high-dimensional data from medical images and reveal previously unrecognized patterns [32-36]. In musculoskeletal imaging, the integration of radiomic features holds promise for advancing the early detection and monitor-

ing of age-related changes in muscle and bone tissue. This study highlights the value of radiomics as a non-invasive, quantitative tool that can provide deeper insights into musculoskeletal health, offering a powerful complement to traditional imaging techniques.

In this study, we examined the correlation between muscle radiomic texture features extracted from T₁-weighted MR im-

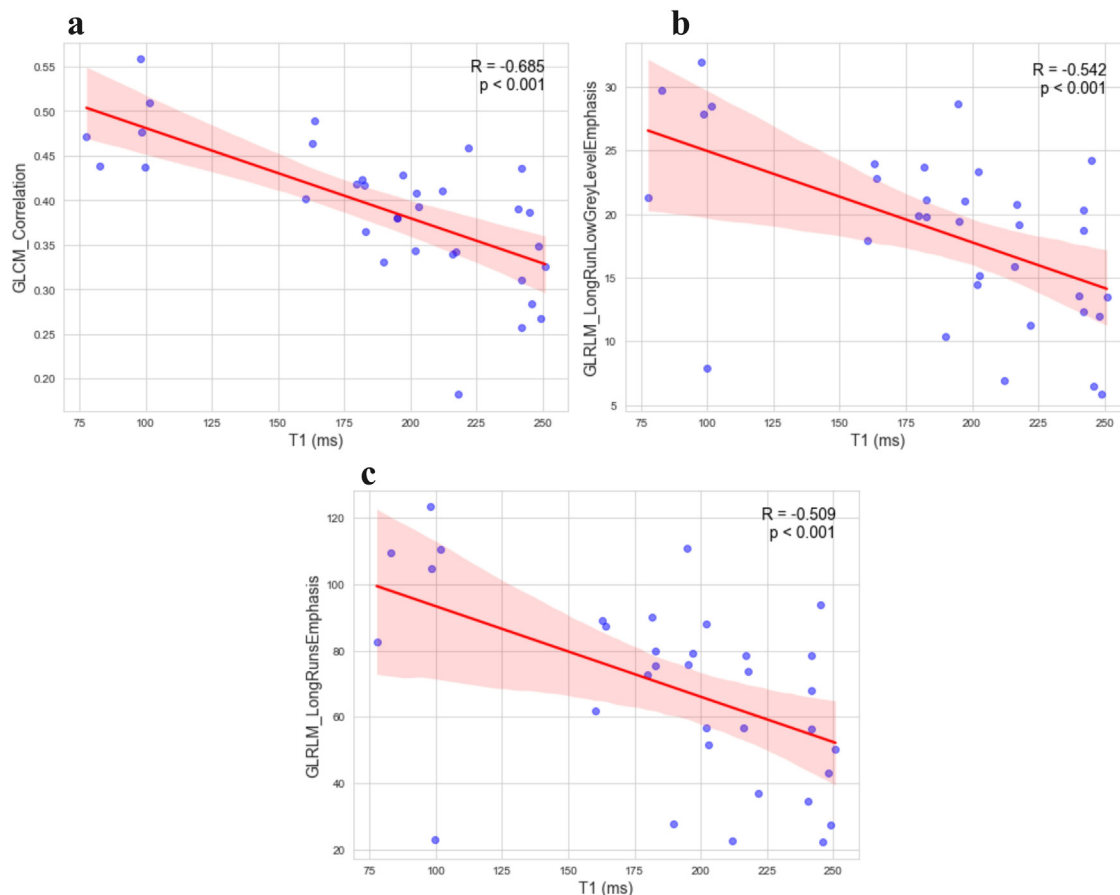


Fig. 5. Correlation of significant texture-based features in the leg muscle with free water T_1 . (a) Gray level co-occurrence matrix (GLCM)-correlation, (b) Gray Level Run Length Matrix (GLRLM) Long-Run Low Grey Level Emphasis, and (c) GLRLM Long-Runs Emphasis.

Table 2

Coefficient of variation (CV %) for significant intensity-based radiomic features, reflecting the variability of feature values across participants.

Intensity_based features	CV (%)
Intensity-based_90th Percentile	1.92
Intensity-based_Interquartile Range	0
Intensity-based_Mean Absolute Deviation	1.92
Intensity-based Robust Mean Absolute Deviation	3.14

ages, cortical bone free water T_1 , and age in healthy adults aged 30–62 years. Radiomic features demonstrated distinct age- and T_1 -dependent patterns, indicating high sensitivity to subtle, age-related tissue alterations that are often undetectable with conventional imaging. Importantly, significant associations between muscle texture characteristics and cortical bone free water T_1 highlight the coupled ageing processes of muscle and bone. These effects were consistently observed across the anterior, posterior, and lateral compartments of the lower leg muscle. Given the well-established biomechanical and biochemical interplay between bone and muscle, alterations in bone structure and composition may reciprocally influence muscle tissue, and vice versa [37,38]. In the present study, radiomic features extracted from leg muscles exhibited significant correla-

tions with both chronological age and cortical bone free water T_1 , thereby supporting our primary objective of identifying radiomics-based biomarkers for characterizing age-related musculoskeletal changes.

The posterior muscle group, particularly the gastrocnemius muscle, showed significant changes in radiomic features, consistent with its known susceptibility to age-related myopathies [39]. Notably, the GLCM Correlation feature demonstrated a strong negative correlation with T_1 ($r = -0.658$, $p < 0.0001$), reflecting decreased gray-level correlation within muscle images as T_1 and age increase. This feature quantifies the probability of pixel pairs with specific gray levels and the linear relationship between their intensities [25,39]. Age-related muscle changes, including atrophy, fiber remodeling, and increased fatty infiltration [1-3,5], are effectively captured by radiomic metrics such as GLCM Correlation, which reflect spatial gray-level gradients.

Considering the clinical complexity of measuring cortical bone free water T_1 via the STE protocol, variations in this radiomic feature may offer a practical surrogate marker for assessing bone-related alterations. The observed compartment-specific radiomic alterations may be partially explained by the functional roles of the involved muscle groups. The posterior compartment, dominated by the soleus and gastrocnemius

muscles, plays a critical role in postural control and locomotion. The soleus muscle, which is predominantly composed of slow-twitch (Type I) fibers, is continuously active during standing and walking, whereas the gastrocnemius contains a higher proportion of fast-twitch fibers and contributes to dynamic movements. Age-related changes in neuromuscular activation, fiber composition, and metabolic demand may therefore differentially affect these muscles, leading to the distinct texture patterns observed in radiomic analysis [5,40,41].

As outlined by Galloway [42], the GLRLM features offer insights into the spatial distribution of consecutive pixels with identical gray-level intensities, calculated across one or more directions in two- or three-dimensional space. In our study, the largest ROI corresponded to this compartment. Anatomically, the soleus muscle, which dominates this ROI, is composed predominantly of slow-twitch (Type I) muscle fibers, with an average proportion of 80 % (range: 64–100 %), whereas the gastrocnemius muscle comprises a lower proportion of slow-twitch fibers (mean: 57 %, range: 34–82 %) [42]. Notably, the gastrocnemius is a biarticular muscle composed of both Type I and Type II fibers, rendering it more susceptible to degeneration due to aging, neurogenic, and myogenic disorders [43]. Therefore, the identification of radiomic features within this compartment that are significantly correlated with age is particularly valuable, as they may reflect underlying muscle composition and microstructural vulnerability to age-related decline.

In the lateral muscle group, two GLRLM features, Long Runs Emphasis ($r = -0.509$, $p < 0.001$) and GLRLM Long Run Low Gray Level Emphasis ($r = -0.542$, $p < 0.001$), exhibited significant inverse correlations with cortical bone free water T_1 . GLRLM Long Runs Emphasis quantifies the distribution of long run lengths in an ROI, where higher values indicate coarser textures characterized by extended sequences of identical gray levels. Conversely, GLRLM Long Run Low Gray Level Emphasis captures the joint distribution of long run lengths and lower gray-level intensities, offering additional insight into the texture and uniformity of muscle tissue [25,39,42]. These features are indicative of the spatial arrangement of consecutive pixels with identical gray levels and provide insights into the muscle's structural changes. Overall, 9.25 % (10/108) and 8.33 % (8/108) of the extracted features exhibited direct or indirect correlations with age and T_1 , respectively. Notably, the GLRLM feature group was the only class to show age-related changes in the lateral compartment, suggesting reduced textural uniformity and increased heterogeneity with aging.

In the anterior muscle compartment, an intensity-based radiomic feature demonstrated the most significant alterations concerning increasing cortical bone free water T_1 ($r = 0.501$, $p = 0.001$), reflecting alterations in low gray-level intensities. Additionally, the NGTDM Complexity feature exhibited notable associations with both age and T_1 ($r = 0.439$, $p = 0.009$ for age; $r = 0.444$, $p = 0.008$ for T_1), indicating increased gray level heterogeneity and image non-uniformity. These texture changes likely correspond to age-related intramuscular fat infiltration, consistent with prior studies [25,39,44]. Collectively,

these findings suggest that such radiomic features may serve as potential biomarkers of muscle microstructural alterations accompanying cortical bone microarchitectural decline, as indicated by free water T_1 , during the aging process [1].

Among the 108 radiomic features extracted from the anterior compartment, the most prominent associations were observed within the Intensity-based and NGTDM categories. As the aging progresses, an increase in the NGTDM Complexity was noted, reflecting greater variability in gray-level intensities and heightened image heterogeneity. This feature quantifies the cumulative differences between a pixel's gray level and the mean gray level of its surrounding neighborhood pixels within a predefined spatial distance [45]. Moreover, several radiomic features from the NGTDM and Intensity-based classes that correlated significantly with age also exhibited correlations with cortical bone free water T_1 . Of particular note, the Intensity-histogram feature "Minimum Histogram Gradient Gray Level" showed a strong correlation with T_1 ($r = 0.501$, $p = 0.03$), further underscoring the interrelated changes in muscle and bone microstructure with aging.

Age-related variations in MR image intensity were associated with changes in muscle fiber composition, with two features showing age-related trends. The Intensity-based Interquartile Range ($r = 0.504$, $p < 0.001$), reflecting the 25th and 75th percentiles of the image intensity distribution, indicates increased heterogeneity in tissue signal [31,39]. Similarly, the Intensity-based Robust Mean Absolute ($r = 0.502$, $p < 0.001$) measures the average deviation of intensity values from the mean, offering a robust estimate of dispersion [31,39]. Both features showed elevated values in muscle tissue with aging, suggesting progressive disruption of tissue uniformity and increased intramuscular structural variability.

Our findings are consistent with those reported by Nodera et al., [46] who demonstrated that texture analysis enables the characterization of anatomical regions based on their texture profiles, thereby providing insights into the underlying microstructural composition of medical images, including skeletal muscle. Their study highlighted the importance of incorporating age-related changes to improve the diagnostic utility of texture-based metrics. By analyzing the medial gastrocnemius muscle in a cohort of healthy individuals aged from their 20 s to late 80 s, they evaluated 283 radiomic features across six categories. They reported that features from the histogram, GLCM, and absolute gradient classes exhibited significant correlations with age in 17–40 % of the parameters. In contrast, none of the run-length matrix features showed significant age-related associations [46]. In our study, however, we observed significant alterations in GLRLM features, particularly in both the gastrocnemius and soleus muscles. Texture changes in the soleus muscle may contribute to age-related radiomic alterations in the posterior compartment.

Previous quantitative MRI studies have demonstrated that aging is associated with increased intramuscular fat infiltration and prolonged T_2 relaxation times, particularly in the calf muscles. These changes reflect alterations in muscle composition and microstructure that precede overt muscle atrophy.

The radiomic features identified in the present study, particularly those reflecting increased signal heterogeneity and altered spatial texture patterns, are consistent with these reported MRI-based biomarkers of muscle aging. Radiomics may therefore provide an indirect, yet sensitive, means of capturing age-related muscle degeneration using standard T1-weighted imaging, without the need for additional quantitative sequences [4,37,47].

These radiomic features may support earlier identification of sarcopenia and fracture risk by capturing subtle muscle and bone microstructural changes that are often missed by conventional assessments such as DEXA. Texture-based muscle MRI metrics may be sensitive to early fat infiltration and muscle atrophy, while associations with cortical bone free-water T1 may reflect early changes related to bone porosity and fracture risk. By incorporating these radiomic features into routine clinical practice, healthcare providers could potentially identify individuals at higher risk for musculoskeletal disorders earlier, facilitating more timely interventions and preventive measures. Moreover, these metrics could be used to monitor the effectiveness of interventions designed to slow the progression of sarcopenia or improve bone health, offering a more nuanced and individualized approach to patient care.

Moreover, beyond their statistical associations, the observed radiomic features may hold important translational value for clinical musculoskeletal imaging. Several texture-based metrics identified in this study reflect increased signal heterogeneity and disrupted spatial organization within muscle tissue, changes that are known to precede overt muscle atrophy and functional decline. As such, these radiomic signatures may serve as early imaging biomarkers of subclinical sarcopenia, potentially enabling risk stratification before measurable reductions in muscle mass or strength occur. Furthermore, given the established link between muscle deterioration, impaired mechanical loading, and bone fragility, muscle-derived radiomic features may provide indirect insight into fracture risk, particularly in individuals who do not meet osteoporosis thresholds based on bone mineral density alone. When integrated into quantitative MRI workflows, radiomic analysis could complement cortical bone free water T1 measurements by offering a non-invasive and spatially resolved assessment of muscle-bone interactions. This integration could enhance musculoskeletal imaging by providing additional biomarkers that complement traditional imaging techniques. Radiomic features can be automatically extracted during MRI acquisition, making it feasible to incorporate them into routine clinical practice with minimal additional effort. The combination of these radiomic signatures with standard MRI measures could improve early detection, risk stratification, and personalized patient management, supporting early preventive interventions aimed at preserving musculoskeletal health.

Musculoskeletal changes associated with aging were detected in individuals under 60 years of age. In this context, the selected age range of the study population warrants further clarification. The restriction of the study cohort to adults aged 30–62 years represents a deliberate focus on preclinical muscu-

loskeletal aging rather than advanced degeneration. While older individuals may exhibit more pronounced structural changes, such alterations are frequently influenced by disease-related processes and functional decline. By targeting a younger-to-middle-aged population, this study demonstrates that radiomic muscle features and cortical bone free water T1 are sensitive to age-related changes well before overt clinical manifestations, underscoring their potential role as early imaging biomarkers.

The relationship observed between muscle radiomic features and cortical bone free water T1 may be explained by both mechanical and biochemical mechanisms governing muscle-bone interactions. Skeletal muscle exerts mechanical loading on bone, which is essential for maintaining bone microarchitecture and strength. Age-related declines in muscle quality and function may therefore contribute to increased cortical porosity and elevated free water content in bone. In addition to mechanical factors, muscle and bone communicate through biochemical signaling pathways involving myokines and osteokines, which regulate tissue remodeling, metabolism, and inflammatory responses [5,7]. Dysregulation of these signaling mechanisms with aging may simultaneously influence muscle microstructure and bone composition, providing a biological basis for the coupled radiomic and T1 changes observed in this study [4].

Several considerations should be taken into account when interpreting the results of this study. The sample size and demographic distribution reflect the scope of the current investigation and may limit the generalizability of the findings. In addition, the single-center, cross-sectional design does not permit causal inference and may be influenced by institution-specific factors. These aspects underscore the importance of future studies incorporating larger, more diverse, and multi-center cohorts to further validate and extend the present findings. Physical activity is a well-recognized factor influencing both muscle and bone health and was not quantitatively assessed in the present study. To mitigate the potential confounding effects of extreme physical activity, participant selection was limited to healthy volunteers without a history of professional or high-intensity athletic training. While this criterion was intended to reduce variability related to exercise extremes, future studies incorporating objective measures of physical activity will be important to more fully characterize its contribution and further refine the interpretation of imaging-derived biomarkers. Moreover, although individuals with known musculoskeletal disorders were excluded to characterize age-related changes in a healthy population, the observed associations may differ in clinical populations such as those with osteoporosis or sarcopenia, where more pronounced structural and compositional alterations are expected. Manual segmentation, although carefully performed by a single trained operator under expert supervision, is inherently subject to observer-related variability. To mitigate intra-observer variability, the segmentation procedure was repeated three times, and the resulting segmentations were averaged for final analysis. However, inter-observer variability was not formally assessed, which may limit

the generalizability of the segmentation reproducibility [40]. Future studies may benefit from the use of semi-automated or fully automated segmentation approaches to further improve reproducibility and efficiency. Moreover, the integration of complementary imaging modalities, such as Dixon-based fat-fraction MRI, and the adoption of longitudinal study designs combining imaging, functional, and biochemical measures, would help to further elucidate the relationships between radiomic features, muscle integrity, and bone health.

Conclusion

This study provides novel insights into the potential of radiomic analysis to characterize musculoskeletal aging. Our results demonstrate that radiomic features extracted from T₁-weighted MR images can sensitively detect age-related changes in muscle tissue, offering a significant improvement over conventional imaging techniques, which often fail to capture such subtle alterations. Notably, several muscle-based radiomic features showed strong correlations with cortical bone free water T₁, emphasizing the close interplay between bone and muscle during the aging process. These findings support the feasibility of using radiomic features as imaging biomarkers for assessing musculoskeletal health. Future studies are warranted to validate these features in larger and more diverse populations and to investigate their applicability in identifying degenerative muscle changes, particularly in the context of age-related conditions such as sarcopenia.

Data availability

The datasets analyzed during the current study are not publicly available for ethical reasons.

Acknowledgments

The authors would like to express their sincere gratitude to Dr. Feraidoon Negahdar for his invaluable guidance and insightful contributions throughout this study.

Supplementary materials

Supplementary material associated with this article can be found, in the online version, at [doi:10.1016/j.jmir.2026.102198](https://doi.org/10.1016/j.jmir.2026.102198).

References

- [1] Akbari A, Abbasi-Rad S, HS Rad. T₁ correlates age: a short-TE MR relaxometry study in vivo on human cortical bone free water at 1.5T. *Bone*. 2016;83:17–22.
- [2] Kumar V, Gu Y, Basu S, Berglund A, Eschrich SA, Schabath MB, et al. Radiomics: the process and the challenges. *Magn Reson Imaging*. 2012;30(9):1234–1248.
- [3] Wilkinson DJ, Piasecki M, Atherton PJ. The age-related loss of skeletal muscle mass and function: measurement and physiology of muscle fibre atrophy and muscle fibre loss in humans. *Ageing Res Rev*. 2018;47:123–132.
- [4] Akbari A, Abbasi-Rad S, HS Rad. T₁ correlates age: a short-TE MR relaxometry study in vivo on human cortical bone free water at 1.5 T. *Bone*. 2016;83:17–22.
- [5] Tieland M, Trouwborst I, Clark BC. Skeletal muscle performance and ageing. *J Cachexia Sarcopenia Muscle*. 2018;9(1):3–19.
- [6] Kirk B, Feehan J, Lombardi G, Muscle Duque G. Bone, and Fat Crosstalk: the Biological Role of Myokines, Osteokines, and Adipokines. *Curr Osteoporos Rep*. 2020;18(4):388–400.
- [7] Cunningham D, Morrison D, Rice C, Cooke C. Ageing and isokinetic plantar flexion. *Eur J Appl Physiol Occup Physiol*. 1987;56(1):24–29.
- [8] Davies C, White M, Young K. Muscle function in children. *Eur J Appl Physiol Occup Physiol*. 1983;52:111–114.
- [9] Hyatt R, Whitelaw M, Bhat A, Scott S, Maxwell J. Association of muscle strength with functional status of elderly people. *Age Ageing*. 1990;19(5):330–336.
- [10] Abbasi-Rad S, Akbari A, Malekzadeh M, Shahgholi M, Arabalibeik H, Saligheh Rad H. Quantifying cortical bone free water using short echo time (STE-MRI) at 1.5 T. *Magn Reson Imaging*. 2020;71:17–24.
- [11] Bijlsma AY, Meskers CG, Westendorp RG, Maier AB. Chronology of age-related disease definitions: osteoporosis and sarcopenia. *Ageing Res Rev*. 2012;11(2):320–324.
- [12] Felisaz PF, Colelli G, Ballante E, Solazzo F, Paoletti M, Germani G, et al. Texture analysis and machine learning to predict water T₂ and fat fraction from non-quantitative MRI of thigh muscles in Facioscapulohumeral muscular dystrophy. *Eur J Radiol*. 2021;134:109460.
- [13] Ager III JW, RK Nalla, KL Breeden, RO Ritchie. Deep-ultraviolet Raman spectroscopy study of the effect of aging on human cortical bone. *J Biomed Opt*. 2005;10(3):034012–034018.
- [14] Almeida M, O'Brien CA. Basic biology of skeletal aging: role of stress response pathways. *J Gerontol A: Biomed Sci Med Sci*. 2013;68(10):1197–1208.
- [15] van Staa TP, Dennison EM, Leufkens HG, Cooper C. Epidemiology of fractures in England and Wales. *Bone*. 2001;29(6):517–522.
- [16] Dalle Carbonare L, Giannini S. Bone microarchitecture as an important determinant of bone strength. *J Endocrinol Invest*. 2004;27(1):99–105.
- [17] Shapiro L, Harish M, Hargreaves B, Staroswiecki E, Gold G. Advances in musculoskeletal MRI: technical considerations. *J Magn Reson Imaging*. 2012;36(4):775–787.
- [18] Cooper D., Kawalilak C., Harrison K., Johnston B., Johnston J. Cortical bone porosity: what is it, why is it important, and how can we detect it? Current osteoporosis reports. 2016;14:187–98.
- [19] Talebi M, Abbasi-Rad S, Malekzadeh M, Shahgholi M, Ardakani AA, Foudeh K, et al. Cortical bone mechanical assessment via free water relaxometry at 3 T. *J Magn Reson Imaging*. 2021;54(6):1744–1751.
- [20] Brunner F, Schmid A, Sheikhzadeh A, Nordin M, Yoon J, Frankel V. Effects of aging on Type II muscle fibers: a systematic review of the literature. *J Aging Phys Act*. 2007;15(3):336–348.
- [21] Nicolau S, Naddaf E. Muscle MRI for neuromuscular disorders. *Pr Neurol*. 2020:27–32.
- [22] Wang Y, Huang Z, Lei J, Lu X, Li S, Wang G, et al. Fatty infiltration in the posterior muscles of the lower extremities as an MRI feature in antimitochondrial antibody-associated myopathy. *Clin Rheumatol*. 2024:1–7.
- [23] Lambin P, Rios-Velazquez E, Leijenaar R, Carvalho S, Van Stiphout RG, Granton P, et al. Radiomics: extracting more information from medical images using advanced feature analysis. *Eur J Cancer*. 2012;48(4):441–446.
- [24] Alderson PO, Summers RM. The evolving status of radiomics. *J Natl Cancer Inst*. 2020;112(9):869–870.
- [25] Mayerhoefer ME, Materka A, Langs G, Häggström I, Szczypiński P, Gibbs P, et al. Introduction to Radiomics. *J nucl med: off publ Soc Nucl Med*. 2020;61(4):488–495.
- [26] Malekzadeh M, Asadi M, Abbasi-Rad S, Abolghasemi J, Hamidi Z, Talebi M, et al. MDCT-QCT, QUS, and DXA in healthy adults: an intermodality comparison. *Med J Islam Repub Iran*. 2019;33:156.

- [27] Nioche C, Orlhac F, Boughdad S, Reuzé S, Goya-Outi J, Robert C, et al. LIFEx: a freeware for radiomic feature calculation in multimodality imaging to accelerate advances in the characterization of tumor heterogeneity. *Cancer Res.* 2018;78(16):4786–4789.
- [28] Baiocco S, Sah B-R, Mallia A, Kelly-Morland C, Neji R, Stirling JJ, et al. Exploratory radiomic features from integrated 18 F-fluorodeoxyglucose positron emission tomography/magnetic resonance imaging are associated with contemporaneous metastases in oesophageal/gastroesophageal cancer. *Eur J Nucl Med Mol Imaging.* 2019;46:1478–1484.
- [29] Van Timmeren JE, Cester D, Tanadini-Lang S, Alkadhi H, Baessler B. Radiomics in medical imaging-“how-to” guide and critical reflection. *Insights Imaging.* 2020;11(1):91.
- [30] Collewet G, Strzelecki M, Mariette F. Influence of MRI acquisition protocols and image intensity normalization methods on texture classification. *Magn Reson Imaging.* 2004;22(1):81–91.
- [31] Nioche C, Orlhac F, Boughdad S, Reuzé S, Goya-Outi J, Robert C, et al. LIFEx: a freeware for radiomic feature calculation in multimodality imaging to accelerate advances in the characterization of tumor heterogeneity. *Cancer Res.* 2018;78(16):4786–4789.
- [32] Bagherpour Z, Safari M, Fadavi P, Haghpanah M, Beigi M. Predicting radiation-induced skin toxicity in breast cancer: a machine learning approach combining radiomic and dosimetric features. *J Med Biol Eng.* 2025;1–12.
- [33] Bagherzadeh S, Fadavi P, Abdollahi H, Arefpour AM, Asgari M, Ahmadabad FG, et al. Vocal cord dysfunction in nonlaryngeal head and neck cancer after chemoradiation therapy: predictive modeling using CT radiomics and machine learning. *Biomed Res Int.* 2025;2025(1):1246604.
- [34] Mansouri Z, Salimi Y, Hajianfar G, Knappe L, Wolf NB, Xhepa G, et al. Potential of radiomics, dosiomics, and dose volume histograms for tumor response prediction in hepatocellular carcinoma following 90Y-SIRT. *Mol Imaging Biol.* 2025;27:201–214.
- [35] Yazdani E, Neizehbaz A, Karamzade-Ziarati N, Emami F, Vosoughi H, Asadi M, et al. Transforming [177Lu] Lu-PSMA-617 treatment planning: machine learning-based radiodosimetrics and swin UNETR using pretherapy PSMA positron emission tomography/computed tomography (PET/CT). *Med Phys.* 2025;52(10):e70030.
- [36] Yazdani E, Neizehbaz A, Karamzade-Ziarati N, Kheradpisheh SR. Explainable artificial intelligence for pneumonia classification: clinical insights into deformable prototypical part network in pediatric chest x-ray images. *J Med Imaging Radiat Sci.* 2025;56(5):102023.
- [37] Bonewald L. Use it or lose it to age: a review of bone and muscle communication. *Bone.* 2019;120:212–218.
- [38] Ferrucci L, Baroni M, Ranchelli A, Lauretani F, Maggio M, Mecocci P, et al. Interaction between bone and muscle in older persons with mobility limitations. *Curr Pharm Des.* 2014;20(19):3178–3197.
- [39] van Griethuysen JJM, Fedorov A, Parmar C, Hosny A, Aucoin N, Narayan V, et al. Computational Radiomics System to Decode the Radiographic Phenotype. *Cancer Res.* 2017;77(21):e104–e7.
- [40] Mayerhoefer ME, Materka A, Langs G, Häggström I, Szczypiński P, Gibbs P, et al. Introduction to radiomics. *J Nucl Med.* 2020;61(4):488–495.
- [41] Wilkinson DJ, Piasecki M, Atherton P. The age-related loss of skeletal muscle mass and function: measurement and physiology of muscle fibre atrophy and muscle fibre loss in humans. *Ageing Res Rev.* 2018;47:123–132.
- [42] Galloway MM. Texture analysis using grey level run lengths. *Nasa Sti/recon Tech Rep N.* 1974;75:18555.
- [43] Patwardhan A, Mukherjee J, Mhatre R, Lanka V, Asranna A, Tiwari R, et al. Muscle MRI-Based Atrophy Pattern Recognition: noTable Findings in a Case of Pathologically Proven Lipid Storage Myopathy. *Ann Indian Acad Neurol.* 2022;25(6):1184–1187.
- [44] Sun C, Wee WG. Neighboring gray level dependence matrix for texture classification. *Comput Graph Image Process.* 1982;20:297.
- [45] Sun C, Wee WG. Neighboring gray level dependence matrix for texture classification. *Comput Vis Graph Image Process.* 1983;23(3):341–352.
- [46] Nodera H, Sogawa K, Takamatsu N, Mori A, Yamazaki H, Izumi Y, et al. Age-dependent texture features in skeletal muscle ultrasonography. *J Med Investig.* 2018;65(3.4):274–279.
- [47] Kirk B, Feehan J, Lombardi G, Duque G. Muscle, bone, and fat crosstalk: the biological role of myokines, osteokines, and adipokines. *Curr Osteoporos Rep.* 2020;18(4):388–400.